Curtis K. Stimpson[1,2]
Mem. ASME
Department of Mechanical and
Nuclear Engineering,
The Pennsylvania State University,
3127 Research Dr,
State College, PA 16801
e-mail: curtis.stimpson@honeywell.com

Jacob C. Snyder
Mem. ASME
Department of Mechanical and
Nuclear Engineering,
The Pennsylvania State University,
3127 Research Dr,
State College, PA 16801
e-mail: jacob.snyder@psu.edu

Karen A. Thole
Mem. ASME
Department of Mechanical and
Nuclear Engineering,
The Pennsylvania State University,
136 Reber Building,
University Park, PA 16802
e-mail: kthole@psu.edu

Dominic Mongillo
Pratt & Whitney,
400 Main Street,
East Hartford, CT 06118
e-mail: dominic.mongillo@pw.utc.com

Effects of Coolant Feed Direction on Additively Manufactured Film Cooling Holes

Gas turbine components subjected to high temperatures can benefit from improved designs enabled by metal additive manufacturing (AM) with nickel alloys. Previous studies have shown that the impact on fluid flow and heat transfer resulting from surface roughness of additively manufactured parts is significant; these impacts must be understood to design turbine components successfully for AM. This study improves understanding of these impacts by examining the discharge coefficient and the effect of the coolant delivery direction on the performance of additively manufactured shaped film cooling holes. To accomplish this, five test coupons containing a row of baseline shaped film cooling holes were made from a high-temperature nickel alloy using a laser powder bed fusion (L-PBF) process. Flow and pressure drop measurements across the holes were collected to determine the discharge coefficient from the film cooling holes. Temperature measurements were collected to assess the overall effectiveness of the coupon surface as well as the cooling enhancement due to film cooling. The Biot number of the coupon wall was matched to a value one might find in a turbine engine to ensure this data is relevant. It was discovered that the flow experienced greater aerodynamic losses in film cooling holes with greater relative roughness, which resulted in a decreased discharge coefficient. The effectiveness measurements showed that the film cooling performance is better when coolant is fed in a co-flow configuration as compared to a counter-flow configuration.
[DOI: 10.1115/1.4041374]

Introduction

Although additive manufacturing (AM) technologies have been around for a few decades, much is still unknown about performance of AM parts. As the impacts of this process on a part's performance become better understood, many new opportunities will arise to use AM for industrial applications. In particular, hot section components of gas turbine engines can benefit from AM because of the increased design freedom it has to offer. Currently, casting is the process of choice for manufacturing hot section turbine components, which means the turbine hardware in use today was designed within the constraints of casting. Removing those constraints by leveraging an additive process can give way to more efficient and effective internal cooling designs that will ultimately lead to further increases in overall turbine efficiency. An additional benefit AM offers is a much faster part turn-around time than conventionally manufactured parts; this has obvious advantages for the product development process.

The authors have previously investigated internal cooling of AM parts made with the laser powder bed fusion (L-PBF) process to understand how heat transfer and fluid flow through microchannels are affected by the AM process [1–3]. Another commonly used turbine cooling technique is manufacturing film cooling holes into hot section components, which help cool the external surfaces of parts. These holes are usually drilled after a part has been cast. Manufacturing film cooling holes with a conventional approach adds an additional process in the production of turbine hardware, which could be eliminated if all features are produced in the same process; this would have obvious manufacturing advantages. Once challenge with making the whole turbine part with AM is that it would result in significant surface roughness in the film cooing holes, which would impact the film cooling performance. Removing the roughness to get a film cooling hole that performs like a conventionally drilled hole may not be economical if at all possible. An understanding of how AM roughness impacts film cooling will allow a turbine designer to account for and possibly leverage the roughness to produce effective cooling designs.

Film effectiveness is frequently studied using a scaled model in a low-speed wind tunnel with a plenum to supply the film cooling holes. Although this ideal case is easy to model computationally and experimentally, rarely will one find an application in gas turbine engines that represents this idealized situation. There are innumerable coolant supply configurations that may exist in an engine. In current designs, flow is usually supplied to film cooling holes from various directions by channels filled with turbulators and impingement jets. Because AM microchannels are just as effective at transferring heat as a cast channel filled with ribs [4], one would only expect an AM film cooling hole to be supplied by an AM microchannel. The authors' previous study examined the performance of film cooling holes made with AM, but only studied coolant delivery from one direction [5]. To increase understanding of how AM affects film cooling performance, the impact on cooling effectiveness due to coolant flow supply direction from an AM channel with film cooling holes was investigated.

The size and morphology of the roughness features must be maintained at engine scale to study their effects, because the roughness is expected to be such a significant driver of the fluid motion in the film cooling hole. For this reason, test coupons

[1]Corresponding author.
[2]Present address: Honeywell, 111 S. 34th St. Phoenix, AZ 85034.

Contributed by the International Gas Turbine Institute (IGTI) of ASME for publication in the JOURNAL OF TURBOMACHINERY. Manuscript received August 8, 2018; final manuscript received August 27, 2018; published online October 8, 2018. Editor: Kenneth Hall.

containing film cooling holes were made at an engine scale from an alloy commonly used in the hot section of turbine engines. The performance of the film cooling holes was assessed using a matched Biot number (Bi) approach, which has been used in numerous previous studies. This approach ensures that overall effectiveness results are directly scalable to engine hardware provided relevant dimensionless parameters are held constant.

Review of Literature

Flow direction and Mach number of fluid approaching both the internal and external sides of a film cooling hole have been shown by many researchers to have an impact on the flow characteristics in and around the hole. Thole et al. [6] investigated the influence of coolant feed velocity on the flow characteristics of a cylindrical film cooling hole in a co-flow configuration. They found that changes in the coolant supply Mach number have a significant impact on the velocity profile at the exit of the film cooling hole. Low Mach numbers (Ma $\approx$ 0) resulted in a high velocity along the windward side of the hole with a separation region at the leeward side right at the entrance. Moderate Mach numbers (Ma $\approx$ 0.3) gave a relatively symmetric velocity profile in the hole. High Mach numbers (Ma $\approx$ 0.5) gave a high velocity along the leeward side of the hole.

Kohli and Thole [7] performed a computational study on the effect of coolant supply flow direction on the adiabatic effectiveness of a shaped film cooling hole. They found that a co-flow configuration resulted in higher adiabatic effectiveness values than counter-flow and plenum supply conditions, which were comparable to each other in performance. Their computational fluid dynamics results showed that the flow in the cooling hole with the counter-flow and plenum configurations was significantly higher along the windward side of the hole. Hale et al. [8] measured adiabatic effectiveness of short cylindrical film cooling holes normal to the surface and at an inclination angle of 35 deg with co-flow and counter-flow feeds. Their results showed that the co-flow configuration resulted in better adiabatic effectiveness than counter-flow. More recently, Wilkes et al. [9] found that higher internal channel Reynolds number reduces the adiabatic effectiveness of the 7-7-7 shaped film cooling hole. This effect is most pronounced at velocity ratios near one than at other velocity ratios. Burd and Simon [10] studied effects of co-flow and counter-flow in short, cylindrical film cooling holes ($L/D = 2.3$) and found little difference in the performance as a result of the supply direction.

In addition to co-flow and counter-flow coolant supply configurations studies, several authors have studied effects of crossflow on film cooling performance compared to plenum or co-flow configurations [7,11–14]. In one of these studies, Saumweber et al. [12] came to the general conclusion that fan-shaped holes are more sensitive to coolant crossflow than round holes, and the effectiveness of both hole shapes are strongly impacted by the internal coolant flow direction.

Another factor that has been found to impact film cooling performance is roughness (both engineered and consequential) in the coolant supply channel and in the film cooling hole. Some researchers have investigated the impact that engineered roughness (i.e., ribs) placed in the coolant supply channel has on film cooling performance [14–17]. They generally found that the roughness features have a significant impact on the performance, which is a function of the rib geometry and location relative to the hole. All studies suggested that the presence of a rib near the hole decreases the film effectiveness relative to a plenum or smooth channel co-flow configuration. Aside from the authors' previous study [5], the impact of roughness as a consequence of the manufacturing process on film cooling performance has only been examined by one study found in public literature. Schroeder and Thole [18] found the roughness in the film cooling hole to have an impact on the film effectiveness. This study generally concluded that larger roughness in the hole ($R_a/D \geq 0.018$) resulted in decreased cooling effectiveness compared to a smooth film cooling hole by as much as 60%.

There are only two papers found in open literature, aside from the authors' previous paper [5], that quantify effectiveness of AM film cooling holes at engine relevant scales [19,20]. However, both of these papers assess the performance of an array of film cooling holes and not an individual row. This paper is unique in that it assesses the effectiveness of a single row of AM film cooling holes fed by coolant in co-flow and counter-flow configurations. Work like this has not yet been published in open literature.

Methods

The importance of maintaining the roughness size and morphology characteristics has been previously mentioned. The experiments presented herein were designed with this in mind. Typical evaluations of film cooling performance employ a low-conductivity material to measure adiabatic effectiveness. This approach could not be pursued here because the roughness formed by an L-PBF machine is unique. Matching the roughness in a material other than metal is currently prohibitively difficult. Therefore, experiments were performed on a set of test coupons that were made out of a metal commonly used for gas turbine components. To ensure that the data would still be relevant and useful to the gas turbine community, a test rig was designed to measure the overall cooling effectiveness of the coupons with a matched Bi and ratio of external to internal heat transfer coefficients, h_∞/h_i. As will be shown in the forthcoming discussion, overall effectiveness measurements in an experiment are representative of what one might observe under engine conditions provided Bi and h_∞/h_i are matched between the two scenarios. The nominal values of these two variables are shown in Table 1. Density ratio (DR), mainstream Mach number, Ma_∞, and internal channel Mach number, Ma_i, maintained in these experiments are also given in Table 1 as well as the film hole Reynolds number range.

Description of Test Coupons. A subset of coupons from the authors' previous study [5] was used for the present study. A cutaway rendering of the coupon design is shown in Fig. 1. These coupons were designed to mimic a piece of gas turbine hardware with film cooling and internal convective cooling. Each coupon contained a coolant supply channel that supplied cool fluid to the film holes and provided convective cooling on the backside of the external wall. The following is a description of the test coupons, how the coupons were produced, and the results of the dimensional measurements made after fabrication.

Each coupon has one row of film cooling holes aligned laterally and is located in the middle of the top surface (see Fig. 1). The film cooling hole shape used for all coupons was the expanded fan-shaped hole that was introduced as a benchmarking shaped film cooling hole by Schroeder and Thole [21]. This hole has a forward expansion angle of 7 deg and an expansion of the same angle in both lateral directions. The metering section has a diameter, D, and a length of 2.5D. The hole is inclined 30 deg relative to the breakout surface and has a total length of 6D. The nominal wall thickness is three-dimensional. Further details of the hole can be found in Ref. [21].

Table 1 Experimental operating conditions

Parameter	Nominal value
Bi	0.1
h_∞/h_i	1.0
DR	1.7
Ma_∞	$\leq$0.3
Ma_i	<0.1
Re_f	5–50 k

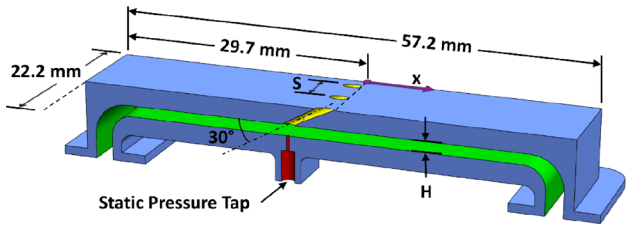

Fig. 1 Test coupon features and dimensions

Film cooling holes of two different diameters were investigated in this study. What will be referred to hereafter as the 1× coupons are those with a film cooling hole diameter of $D = 0.38$ mm, and those referred to as the 2× are coupons have a film hole diameter of $D = 0.76$ mm. The two hole sizes are geometrically scaled versions of each other. These specific hole diameters were selected to represent the general upper and lower bounds of film cooling holes generally found in aircraft turbine engines. The spacing between each hole, S, was 6D and the holes stretched from one side of the coupon to the other. There was sufficient space for five holes in the 2× coupons and nine holes in the 1× coupons.

All coupons were made in a single build using a state-of-the-art L-PBF machine. They were made from a nickel-chromium-iron-molybdenum-based powdered alloy [22] with a composition identical to that of Hastelloy® X. The material scaling and beam offset parameters were established by building a calibration block in a separate calibration build. All other machine parameters were those recommended by the L-PBF machine manufacturer for the specific alloy used [23]. Thermal properties of this material are identical to those of the wrought alloy. Duplicates of each coupon design were built at two different build directions; these are illustrated in Fig. 2. This was done to assess the performance at a favorable build direction (i.e., hole axis aligned vertically) and an unfavorable build direction (i.e., hole axis angled at 21 deg above horizontal) with respect to the best net shape and minimal roughness of the film cooling holes. Assessing the effect of build direction is important, as most turbine components do not have all holes aligned at the same angle. Therefore, building a part will likely result in film cooling holes oriented in many directions.

After the coupons were built, the build substrate and attached coupons were removed from the L-PBF machine. Excess powder in the channels of the coupons was removed, and the parts were heat treated while still attached to the build plate to relieve residual stress resulting from the manufacturing process. The test coupons were then separated from the build substrate, support material was removed, and the top surface of the coupon was smoothed. This smoothing was performed to simulate what might actually be done in application of an AM turbine component. External roughness causes unnecessary aerodynamic losses and can be removed easily with conventional subtractive manufacturing processes (e.g., abrasive blasting, subtractive machining, tumble finishing, etc.). An additional reason for smoothing the surface was to produce a predictable fluid boundary layer unaffected by roughness.

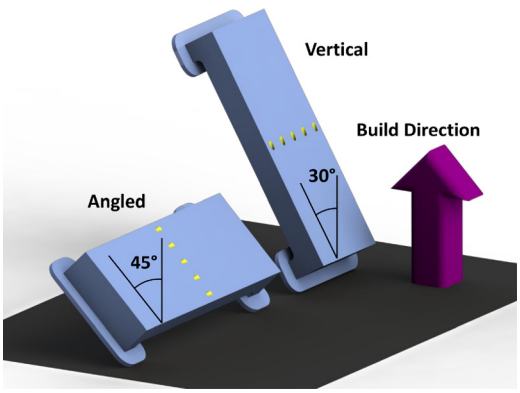

Fig. 2 Coupon orientation during build showing vertical build direction and angled build direction

The final step in preparing the coupons for testing was adding a thin layer of black paint to the top surface of the coupon to reduce reflectivity and increase the radiative emissivity, which is important for thermographic measurements. The insides of the film cooling holes were kept free from paint to ensure the roughness morphology was not altered.

Details of the five coupons investigated here are provided in Table 2. The coupon name is listed in the top row of the table. The first part of the name denotes the size of the film cooling holes in the coupon. The second denotes the build orientation of the film cooling holes with the exception of the 1× electrical discharge machining (EDM) coupon. The film cooling holes in this coupon were made with EDM as a benchmark for comparing conventionally manufactured film cooling holes to AM film cooling holes. Also listed in the table are the geometric design specifications for each coupon. These include the film cooling hole metering section diameter, D, the hydraulic diameter of the coolant supply channel, $D_{h,i}$, the wall thickness separating the coolant and the mainstream flow, t, and the minimum flow area of the film hole, A_{min}. An estimated R_a/D is also supplied in the table. This was based on roughness measurements from the authors' previous work [3]. An estimate is presented because accurate, quantitative roughness measurements on the AM film cooling holes are unattainable with techniques currently available. Attempts to measure and quantify the roughness in the film holes with white light interferometry would have resulted in large uncertainties, and such data are likely less accurate than an estimate made using the previous measurements. However, qualitative images of the roughness were collected and are presented in the Results and Discussion section.

Although tolerances of parts produced by L-PBF are generally very good in terms of an absolute reference, slight dimensional inaccuracies can have a large impact on the relative error of small internal channel dimensions. Additionally, significant roughness can alter the effective location of a surface. The authors have learned through previous work that it is of vital importance to characterize the geometric scales accurately. Poor characterization or use of nominal values will result in significant error in the results. Therefore, the five coupons' geometry was measured with a computed tomography scanner. The computed tomography scanner and associated post processing software can accurately locate the surfaces of the part with precision as good as 3–4 μm [24]. The results of this are also presented in Table 2 as the measured values. A general comparison of these will show that the coolant supply channel is smaller than intended, and the thickness of the wall is very close to the design specification. The average minimum area, $A_{min,avg}$, of the film cooling holes represents the average of the minimum areas from all film cooling holes. The average is presented because there is variation in the minimum area from one film cooling hole to another in the same coupon. Further details of the characterization results, including cross-sectional images of the holes, have been presented previously by Stimpson et al. [5].

Experimental Setup. The coupons were tested in a rig developed for a previous study done by Stimpson et al. [5]. A cut-away view of the rig is given in Fig. 3. The rig was designed to supply coolant to the internal channel while simultaneously flowing ambient temperature air over the top surface of the coupon. Some of the coolant supplied to the channel exited through the film cooling holes, and the remainder exited the other end of the coupon. This provided both film cooling and internal cooling. The coolant could be supplied to the coupon from either the upstream side (relative to the mainstream flow direction) or the downstream side.

Table 2 Test coupon dimension specifications and measurements

Coupon Name	1× EDM	1× Vertical	1× Angled	2× Vertical	2× Angled
Symbol	△	▲	△	●	○
Number of film holes	9	9	9	5	5
Design D (mm)	0.381	0.381	0.381	0.762	0.762
R_a/D (estimated)	< 0.003	0.02	0.04	0.01	0.02
Design $D_{h,i}$ (mm)	2.45	1.26	1.26	2.45	2.45
Measured $D_{h,i}$ (mm)	1.78	0.93	0.72	2.10	1.89
Design t (mm)	1.14	1.14	1.14	2.29	2.29
Measured t (mm)	1.18	1.17	1.20	2.30	2.32
Design A_{min} (mm^2)	0.114	0.114	0.114	0.456	0.456
Measured $A_{min,avg}$ (mm^2)	0.107	0.076	0.0278	0.405	0.281
Build direction	Angled	Vertical	Angled	Vertical	Angled

This allows for testing effectiveness of the coupon surface in a co-flow configuration (i.e., coolant and mainstream flowing in the same direction) or in a counter-flow configuration (i.e., coolant and mainstream flowing in opposite directions).

The opening of the mainstream channel was 9.5 mm high and 25.4 mm wide. The channel was sufficiently long upstream to produce aerodynamically developed turbulent flow. The mainstream channel was supplied with dry, compressed air at a nominal 20 °C and 4 bar. Flow rate of the air was measured with a turbine flow meter installed upstream of the rig. A pressure regulator downstream of the flow meter and upstream of the rig was used to set the operating pressure of the mainstream. A valve downstream of the rig worked in tandem with the pressure regulator to control pressure and flow rate through the channel.

The part labeled in Fig. 3 as the *Coupon Feed with Integrated Instrumentation* was made with AM using a stereo lithography apparatus (SLA). The flexibility and design freedom of AM allowed for a compact, multifunctional design that simplified instrumentation. The SLA part held the coupon in place, so the surface of the coupon was flush with the interior wall of the mainstream channel. It also directed coolant flow into the coupon channel. Numerous channels and holes were printed directly into the SLA part into which thermocouples and pressure taps were installed. Three thermocouples were installed at the inlet and three were installed and exit of the coupon coolant channel. Pressure taps upstream and downstream facilitated pressure measurements of the coolant. Additional pressure taps were installed into the bottom coupon wall directly below the inlet of the film cooling holes to measure static pressure at the inlet of the film cooling holes. The relatively low dynamic pressure in the coolant channel during experiments minimizes any uncertainty that might arise in the pressure measurement due to surface roughness or flow direction.

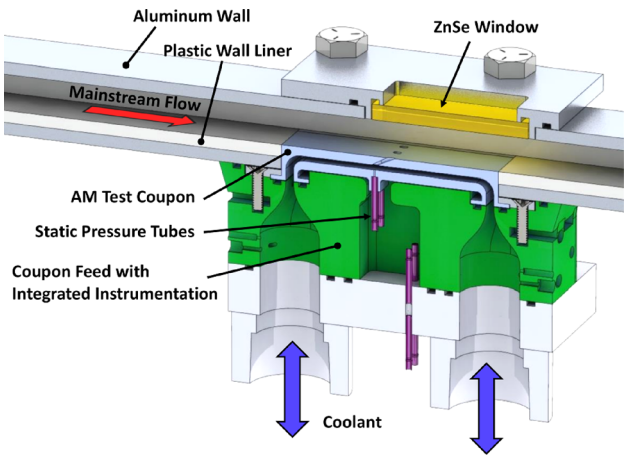

Fig. 3 Test rig from Stimpson et al. [5] used for this study

The fluid used for the coolant was refrigerated carbon dioxide (CO_2) fed from a liquid dewar. The liquid was evaporated and warmed to a temperature around −5 °C before it entered the coupon. The combination of the cooler temperature and the higher molecular weight of CO_2 resulted in a density ratio, $DR = \rho_c/\rho_\infty$, of about 1.7.

Measuring the flow rate of coolant exiting the film holes and the flow rate of the remaining coolant exiting the outlet of the coupon was vital for data reduction. The portion of the coolant flow that exited the channel (i.e., did not exit through the film cooling holes) was measured using a laminar flow element placed after the exit of the coupon. Because the flow rate of coolant exiting the film cooling holes was significantly less than the total flow rate of coolant entering the coupon, an attempt to measure the film cooling flow rate using a mass balance of the inlet and exit streams of the coupon would have resulted in an unacceptably high uncertainty. An alternative approach was pursued for this study where the flow rate through the film holes was characterized as a function of pressure ratio in a separate experiment. The flow rate, reduced into the form of a flow parameter (FP), was characterized over a range of pressure ratios with the exit of the coupon closed off. Appropriate instrumentation enabled accurate measure of flow rate and pressure drop across the film cooling holes. The pressure ratio versus flow parameter data was then used to determine the film cooling flow rate during heat transfer testing.

Coolant channel Reynolds number, Re_i, on the downstream portion of the channel (relative to the mainstream flow direction) was held constant at a value of 14k for all experiments. Because overall surface effectiveness is a function of the internal heat transfer coefficient, h_i, the external heat transfer coefficient, h_∞, and the thermal resistance of the coupon wall, it was important to keep these three factors constant to isolate the effect of film cooling. Maintaining a constant Re_i for all conditions and coolant supply directions ensured a constant h_i, so comparisons could be made between different data points. The magnitude of h_i was determined from a correlation for convective heat transfer in AM channels previously presented by Stimpson et al. [3]. Because Re_i was matched on the downstream portion of the coupon, the mass flow ratio of coolant that exited the film cooling holes to the total mass flow entering the coupon varied from nearly 100% for the 2× vertical coupon at the highest M tested and 7% for the 1× angled coupon at the highest M tested.

The value of h_∞ was estimated using a formulation for developing flow between two parallel flat plates with one side heated by a constant surface heat flux. This model was obtained from Kays et al. [25] and was used in the authors' previous study [5]. The external heat transfer coefficient was assumed identical for cases with and without film cooling. This is justified for analyzing specially averaged values because h_∞ changes only in the region near the film cooling hole [26]. Stimpson et al. [5] found that despite the uncertainty of using a correlation, the repeatability is good and does not affect comparative analysis of the effectiveness data when h_∞ is held constant as was done in both the previous and

present studies. Further details of this model can be found in Ref. [5]. It is important to note that Bi was held constant between the 1× and 2× coupons by adjusting h_∞ because the coupon wall thickness and thermal conductivity were fixed.

The boundary layer in the mainstream channel was assumed to be fully developed. The boundary layer thickness, displacement thickness, and the momentum thickness were approximated as $\delta/D = 6.3$, $\delta^*/D = 0.78$, and $\theta/D = 0.63$ for the 2× coupons assuming a 1/7th power turbulent profile. These parameters scaled by a factor of two are the boundary layer parameters for the 1× coupons.

Once Bi, h_∞/h_i, and DR were matched to the values in Table 1, all flow rates, temperatures, and pressures were held constant before thermal images were collected to ensure the results were steady-state measurements. Thermal images of the coupon surface were collected with an infrared (IR) camera through a zinc selenide (ZnSe) window. ZnSe has a nearly constant transmissivity of 0.7 in the infrared band making it the most ideal material for a viewing window. A series of ten thermal images were collected and averaged to ensure the final result represented the average, steady-state value.

Data Analysis Methods. The film cooling hole flow and pressure data collected in preliminary flow experiments was reduced into a dimensionless, $\mathrm{FP} = \dot{m}_f(\mathrm{RT_c})^{0.5}/P_c A_c$, and a pressure ratio, $\mathrm{PR} = P_c/P_\infty$. Putting the data in this form compensates for any variation in temperature, operating pressure, or fluid type. Therefore, collecting the preliminary data with air at ambient temperature produces the same result as with cooled CO_2. FP data from the preliminary experiments were used to determine the flow rate of coolant through the film cooling holes in the heat transfer experiments by measuring the drop in pressure across the film cooling hole and interpolating the FP versus PR results.

The FP versus PR data can also be evaluated in the form of a discharge coefficient, C_d, which is a ratio of actual mass flow rate to ideal mass flow rate through a film cooling hole. The formulation of C_d presented by Gritsch et al. [27] was used here with slight modifications. The modified version is given in Eq. (1) in terms of total mass flow rate through all film cooling holes, $\dot{m}_f$, coolant supply total pressure, $P_{t,c}$, mainstream static pressure, P_∞, coolant stagnation temperature, $T_{t,c}$, the number of film cooling holes, N, and the average of the measured minimum flow areas from each hole in a given coupon, $A_{\mathrm{min,avg}}$. The other constants, R and γ, are the gas constant and ratio of specific heats, respectively. The bar is placed over C_d in Eq. (1) to denote that this is the average C_d for all the film holes in a given coupon

$$\overline{C_d} = \frac{\dot{m}_f}{P_{\mathrm{t,c}}\left(\frac{P_\infty}{P_{\mathrm{t,c}}}\right)^{\frac{(\gamma+1)}{2\gamma}}\sqrt{\frac{2\gamma}{(\gamma-1)RT_{\mathrm{t,c}}}\left[\left(\frac{P_{\mathrm{t,c}}}{P_\infty}\right)^{\frac{(\gamma-1)}{\gamma}}-1\right]}\mathrm{NA_{min,avg}}} \tag{1}$$

During analysis of the IR measurements, the surface temperature measured with the IR camera was adjusted using a calibrated radiative heat transfer equation. This equation incorporated the surrounding temperatures, emissivities, transmissivities, and a spatially resolved view factor for the coupon surface. The radiative parameters such as ZnSe transmissivity, surface emissivity of the painted coupon, surface emissivity of the channel walls, etc. were selected through a series of calibrations where the coupon surface temperatures were known. The calibrated wall temperature data were normalized according to Eq. (2), where T_w is the wall temperature of the coupon, T_∞ is the mainstream static temperature, and T_c is the reference coolant static temperature. Because both co-flow and counter-flow data were being assessed in this study, using the temperature at a constant location for both flow directions was not logical. Instead, the coolant reference temperature was selected to be the temperature of the coolant at the point it entered the region of interest (i.e., the downstream half of the coupon). For the counter-flow tests, the reference coolant temperature was that of the coolant entering the coupon. The reference coolant temperature for the co-flow tests was the temperature of the coolant halfway down the channel, which corresponds to the inlet of the film cooling holes.

$$\phi = \frac{T_\infty - T_w}{T_\infty - T_c} = \frac{1-\chi\eta}{1+\mathrm{Bi}+h_\infty/h_i} + \chi\eta \tag{2}$$

An alternative form of the overall effectiveness is also given in Eq. (2) which can be derived using a one-dimensional analysis of heat transfer through the coupon wall [28]. This form of overall effectiveness is in terms of Bi, h_∞/h_i, adiabatic or film effectiveness, η, and coolant warming factor, χ. When Bi and h_∞/h_i are matched to the engine conditions, one can expect the resulting effectiveness measurements to represent engine effectiveness values given that all flow boundary conditions are also matched and χ is not significantly different.

Augmented effectiveness, ϕ/ϕ_o, was calculated to isolate the impact of film cooling from that of internal cooling. The effectiveness of the coupon surface with the same internal convection and no film cooling, ϕ_o, is used to normalize the effectiveness data collected at various film flow rates. Evaluating this ratio using the definition given in Eq. (2) shows that it scales with the product of adiabatic effectiveness, η, and coolant warming factor, χ, as seen in Eq. (3). Examining this ratio gives insight into the adiabatic film effectiveness without directly measuring it

$$\frac{\phi}{\phi_o} = 1 + \chi\eta\left(\mathrm{Bi} + \frac{h_\infty}{h_i}\right) \tag{3}$$

Measurement Uncertainty. An uncertainty analysis was carried out according to the root sum squared method described in Ref. [29] to assess the accuracy of the experimental results. The parameters analyzed for uncertainty were C_d, DR, Bi, h_∞/h_i, M, φ, and φ/φ_o. The uncertainty of C_d was driven by the measurement of A_{min}, which was largest with the 1× coupons. At $\mathrm{PR} > 1.1$, the uncertainties of C_d for the 2× and 1× AM holes were, respectively, ±0.05 and ±0.10. However, these data were highly repeatable and repeatability uncertainty is less than ±0.01.

Density ratio was only a function of the temperature measurements and was certain to within ±3%. The uncertainty in Biot number of the coupon wall was much higher because it depended primarily upon h_∞, which has a large uncertainty associated with it due to the use of a correlation. Bi is accurate to within ±28%. The correlations used for h_∞ and h_i inherently resulted in high uncertainty for h_∞/h_i, which was evaluated to range between 15–30% with the major contributor being the uncertainty in h_i. The uncertainty in M was calculated to be ±18% for the 1× coupons and ±11% for the 2× coupons. A_{min} played a significant role in the uncertainty of M. The dependent variable under investigation in this study, φ, has an uncertainty of ±7% at high M and ±9% at low M. This resulted in an uncertainty of φ/φ_o of 11% and 13% at high and low M, respectively.

Although the absolute uncertainties of Bi and h_∞/h_i are large, the parameters affecting these values, such as mass flow rate and pressure, were accurately controlled. Therefore, the repeatability of Bi and h_∞/h_i was adequate for each hole size. The data collected with one 1× coupons can reliably be compared to the other 1× coupons. The same is true for the 2× coupons.

Nearly all measurements of φ for all coupons are within the absolute uncertainty of each other, as will soon be seen. However, establishing the repeatability of the experiments allows for reliable conclusions of the trends in the data. All data presented hereafter has been repeated at least once, and the repeatability of the experiments produces a value of φ that varies between 2–3%. This means that the results can be analyzed on a comparative basis

with good confidence. Consequently, φ/φ_o is repeatable to within ± 0.05 for all data and lends to reliable comparative analysis.

Results and Discussion

The discussion of results is divided into two sections. First, the results from the flow tests will be presented. The flow results for each coupon were reduced to a C_d. The effect of mainstream Mach number was investigated for one of the AM coupons, and the corresponding results are reported in the first section as well. In the second section, cooling effectiveness results for the two different coolant supply flow directions are presented in the form of an augmented overall effectiveness. Area averaged results are compared for different mass flow rates of film cooling.

Discharge Coefficient. C_d results of the film cooling holes of all coupons are plotted as a function of PR in Fig. 4, where $Ma_\infty = 0$ and $Ma_i < 0.1$. The coupon with the highest C_d is the $1\times$ EDM coupon. The reason for this is that the EDM process produces a smoother surface finish than the AM process. A comparison of the roughness between the EDM hole and the $2\times$ AM holes can be seen qualitatively in the scanning electron microscope micrographs in Fig. 5. The EDM hole (Fig. 5(*c*)) is much smoother than either of the $2\times$ AM holes (Figs. 5(*a*) and 5(*b*)).

The data from the two $2\times$ coupons presented in Fig. 4 show the holes on these coupons produce a lower C_d than the holes in the $1\times$ EDM coupon. As might be expected from the two $2\times$ coupons, the one with the holes built in the vertical direction had a slightly higher discharge coefficient than the one with the angled holes, although this is not conclusive considering the uncertainty. This result is attributed to the larger relative roughness in the angled holes. Figures 5(*a*) and 5(*b*) shows the difference in roughness between the two build directions. This figure also shows that the net shape of the metering section is different between these two holes. Remember that C_d accounts for the area of the holes so the decreased flow area of the $2\times$ angled film holes compared to the $2\times$ vertical holes should have no impact on C_d. As is also seen in Fig. 4, the roughness of the $2\times$ angled film hole is greater than the $2\times$ vertical especially on the upper left-hand region of the hole. This region was a downward facing surface with respect to the build direction; downward facing surfaces are known to be much more rough than upward facing or vertical surfaces.

The discharge coefficients of the $1\times$ film holes are much lower than those of the $2\times$ film holes. This is also attributed to the roughness. The absolute roughness of all coupons is the same regardless of the size of the film cooling holes. Therefore, the relative roughness of the $1\times$ film holes will be significantly greater than the roughness of the $2\times$ film holes. This is believed to be the reason for the dramatic decrease in C_d. A comparison of C_d between the two $1\times$ AM coupons again shows that the vertically built film cooling holes perform better than the angled, which is attributed to differences in relative roughness due to the build direction. Detailed characterization of the $1\times$ coupons done by Stimpson et al. [5] showed that the roughness was so large in the $1\times$ angled holes that the flow area of some holes was nearly blocked entirely, which contributed to the particularly low C_d.

Also shown on Fig. 4 is data from Whitfield et al. [30] who examined C_d for a larger-scale, smooth film cooling hole of the same shape in a low-speed wind tunnel. Theirs is the only paper that has previously characterized flow through this hole shape. The pressure ratios of their data ranged between 1.00 and 1.01. Because of this small range in PR, all their C_d data were averaged together and presented as one data point on the graph. This was done because the variation in C_d between $1.00 < PR < 1.01$ is smaller than the size of the symbol on the figure. The impacts of the scaling on C_d are unknown for this hole; there may be PR effects that are not visible in their data. However, their measured C_d is similar to those measured in this study.

Gritsch et al. [27] characterized C_d of cylindrical and fan-shaped film cooling holes at $Ma_\infty = 0.0$, 0.3, 0.6, and 1.2 and at $Ma_i = 0.0$, 0.3, and 0.6. Their work showed that Ma_∞ has a significant impact on C_d for $Ma_\infty > 0.3$ and for $Ma_i > 0.2$ with their hole geometry. Because the experiments in this study relied on the PR to determine the film flow rate, it was important to assess any impact due to Ma. Ma_i was small (<0.1) for all flow conditions, so these effects were assumed to be insignificant. The results from Gritsch et al. [27] justified this assumption. However, an assumption that Ma_∞ has an insignificant impact on the C_d necessitated further validation. An experiment was carried out to quantify the influence of Ma_∞ on C_d. Results of C_d and PR for $Ma_\infty = 0.0$, 0.3, and 0.6 are given in Fig. 6 for the $2\times$ vertical coupon and the fan-shaped geometry from Ref. [27]. The data from the $1\times$ EDM at $Ma_\infty = 0.0$ are also included for comparison.

There are three major observations that can be seen in Fig. 6. First, C_d of the $1\times$ EDM hole and the fan-shaped hole from Ref. [27] are very similar at $Ma_\infty = 0.0$. Second, the impact of Ma_∞ is very similar between the fan-shaped hole and the $2\times$ vertical hole. At low PR, both exhibit a small difference between $Ma_\infty = 0.0$ and $Ma_\infty = 0.3$ and a much larger difference between $Ma_\infty = 0.0$ and $Ma_\infty = 0.6$. This suggests that Mach number effects may not be dependent on roughness in film cooling holes. The third important observation is that the difference in C_d between $Ma_\infty = 0.0$ and $Ma_\infty = 0.3$ is small enough that it lies within the experimental uncertainty. This says that the flow rate of the film for $Ma_\infty \leq 0.3$ is not a function of Ma_∞, and the same FP versus PR data can reliably be used to determine the flow rate of the film.

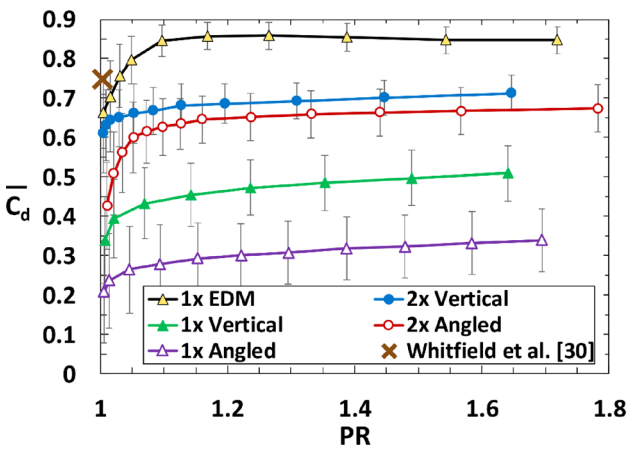

Fig. 4 Discharge coefficient of EDM and AM coupons where $Ma_\infty = 0$ and $Ma_i < 0.1$

Effectiveness Results. Surface temperature measurements were collected from the downstream portion of each coupon using IR thermography. The temperature results were put into the form of an overall effectiveness, φ. Some overall effectiveness results for the $2\times$ vertical coupon are shown in Fig. 7. The top two images in the figure show contours of φ with no film cooling (i.e., $M = 0.0$) in the co-flow configuration (Fig. 7(*a*)) and in the counter-flow configuration (Fig. 7(*b*)) from $-3 < x/D < 30$. Recall that Re_i and h_∞ are constant between these two cases. The differences observed in the contours are due to the flow direction of the coolant. The length of the $2\times$ coupons from the exit of the film cooling hole to the edge is about $x/D = 36$, and the 90 deg turn occurs at about $x/D = 33$; these relative locations are illustrated in Fig. 8. The data shows that the temperature is nearly constant over this region in the co-flow configuration because the internal flow has developed aerodynamically and does not result in a significant change in surface temperature. On the other hand, the effectiveness is increasing in the x-direction in the counter-flow configuration. This is the result of the coolant impinging on the internal surface after it exits the 90 deg turn. The $1\times$ coupons do not

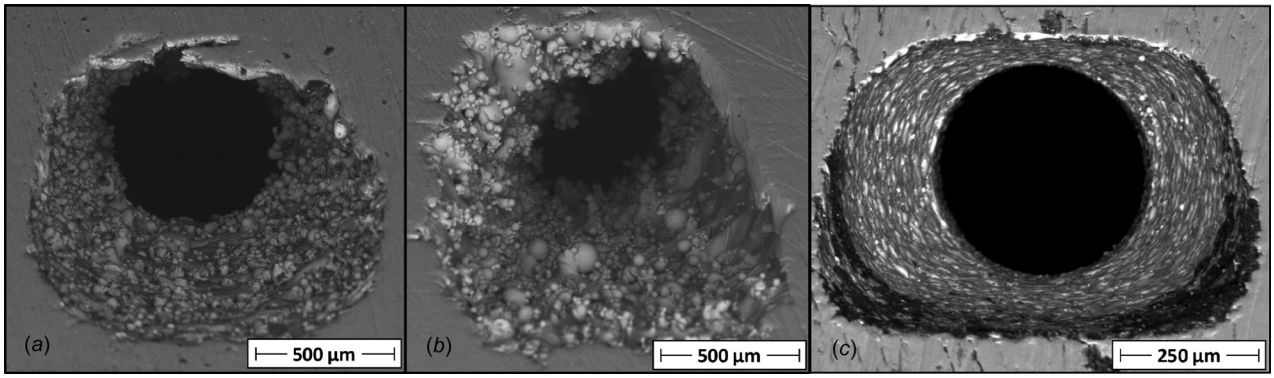

Fig. 5 Micrographs of film cooling holes (*a*) at 2× scale made in the vertical build direction, (*b*) 2× scale made in the horizontal build direction, and (*c*) 1× scale drilled with EDM

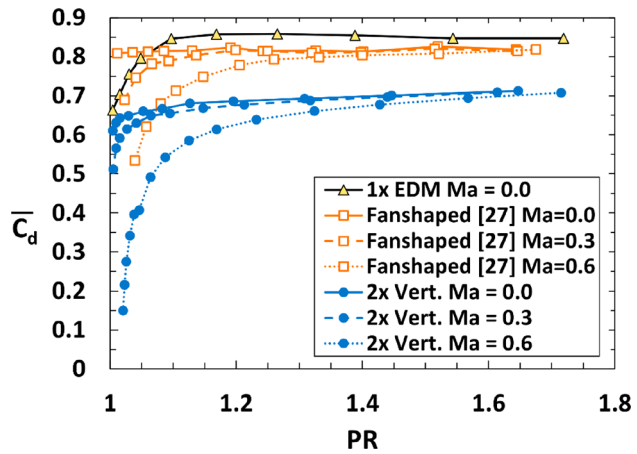

Fig. 6 Discharge coefficient, C_d, of EDM and 2× vertical coupon with compared to C_d of a fan-shaped hole from Gritsch et al. [27]

experience such significant differences in φ for $M = 0.0$ for $-3 < x/D < 30$ because the 90 deg turn occurs at $x/D = 65$. The 1× coupon data were only analyzed from $-3 < x/D < 30$ in the interest of consistency in analysis between the 1× and the 2× coupons. Over this region for the 1× coupons, φ experienced a small change in the streamwise direction for both the co-flow and counter-flow configurations.

Figures 7(*c*) and 7(*d*) shows φ for the 2× vertical coupon with film flowing through the holes at $M = 1.0$. One can see that the distinct film traces extend to nearly $x/D = 20$ for both co-flow and counter-flow configurations. The co-flow configuration has the highest effectiveness right at the exit of the film cooling holes that decreases with increasing x/D. The counter-flow configuration has similar φ contours around the holes with slightly different magnitudes. The effectiveness of the counter-flow configuration also decreases with increasing streamwise distance, but at $x/D \approx 15$, the effectiveness begins to increase again due to the internal cooling.

In order to make comparisons of film cooling performance, an area-averaged augmented effectiveness, $\bar{\bar{\varphi}}/\bar{\bar{\varphi}}_o$, was calculated for each condition. As described previously, the augmented overall effectiveness is the effectiveness of the surface of a coupon divided by the effectiveness of same coupon without film cooling

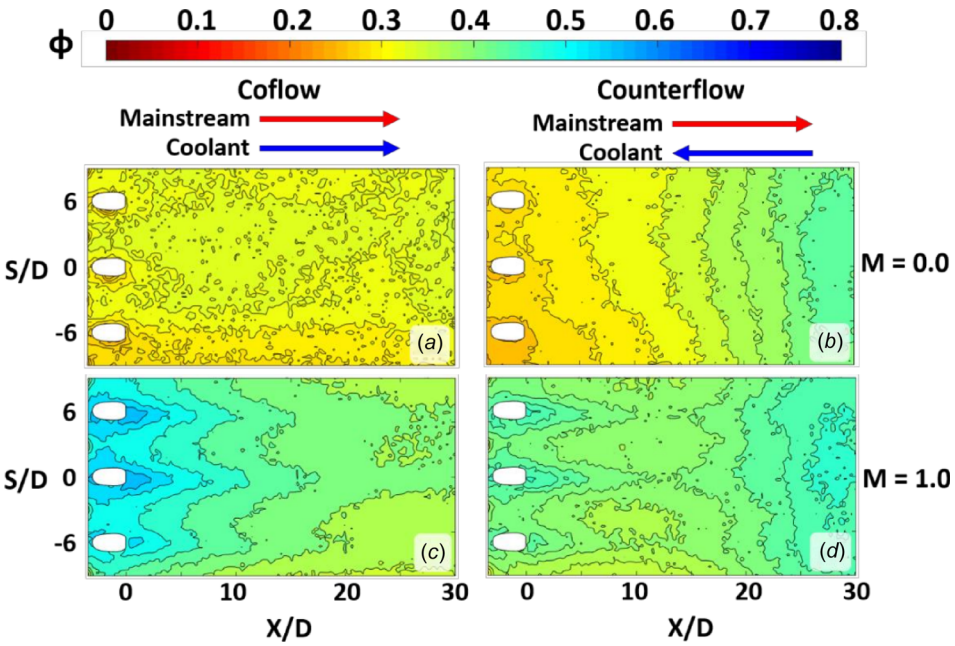

Fig. 7 Overall effectiveness of 2× vertical coupon at $Re_i = 14{,}000$ with $M = 0.0$ (a,b) and $M = 1.0$ (c,d)

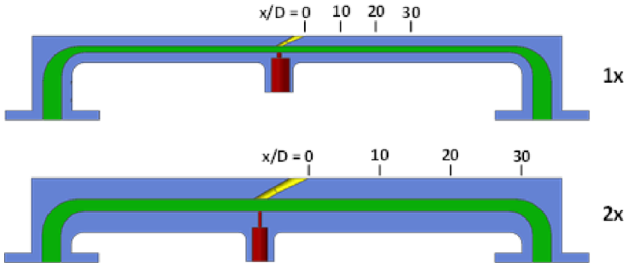

Fig. 8 Cross-sectional view of 2× coupon showing *x/D* scale relative to coupon features

flow. This quantity is proportional to the adiabatic effectiveness as expressed in Eq. (3). The area over which the overall effectiveness was evaluated extends from $0 < x/D < 30$ and $-9 < S/D < 9$, where the datum $S/D = 0$ was the symmetry line of the center film cooling hole.

The values of $\bar{\bar{\varphi}}/\bar{\bar{\varphi}}_o$ for the three 1× coupons are shown as a function of blowing ratio, M, in Fig. 9, where M is calculated using the measured average minimum area, $A_{min,avg}$, given in Table 2. Considering the findings of Schroeder and Thole [18], who showed that smooth film cooling holes result in higher adiabatic effectiveness than rough holes, one would expect the 1× EDM coupons to give the highest effectiveness results. Figure 9 shows that this is indeed the case for the 1× coupons in the co-flow configuration. The augmented effectiveness also follows the same trends with respect to M that was reported in Ref. [18]; there is a sharp increase in $\bar{\bar{\varphi}}/\bar{\bar{\varphi}}_o$ for $M < 1$ and a decrease for $M > 2$ as the jet becomes detached from the surface. However, the decrease in effectiveness for $M > 2$ is not as great as what was reported in Ref. [18]. The co-flow results of all three 1× coupons are also in agreement with the previous measurements of effectiveness with these same coupons [5]. The successive increase in roughness of the 1× EDM, the 1× vertical, and the 1× angled holes give a strong decrease in film effectiveness. This confirms the significant role roughness plays on the performance of film cooling holes.

Kohli and Thole [7] predicted that the film effectiveness of a fanshaped hole is higher when it is fed in a co-flow configuration than a counter-flow configuration. This prediction is corroborated with the data from the 1× EDM coupon. The co-flow configuration has higher augmented effectiveness than the counter-flow configuration. Detailed flow modeling in the film hole metering and diffuser sections done by Kohli and Thole [7] showed that velocities along the windward side of the film cooling hole were much greater in the counter-flow configuration. This phenomenon is believed to be the result in greater detachment of the film jet because of the increased momentum of the coolant in the hole. The augmented effectiveness results of the AM film holes shown in Fig. 9 do not indicate any significant difference because of the coolant supply direction within the repeatability uncertainty. This is likely due to the in-hole roughness mixing out any high velocity regions that might otherwise exist if the holes were smooth. As shown in Ref. [5], the roughness features in the 1× AM holes protrude far into the flow and would presumably cause high levels of mixing in the hole.

$\bar{\bar{\varphi}}/\bar{\bar{\varphi}}_o$ is given for the two 2× coupons as a function of blowing ratio, M, in Fig. 10, where M is calculated using the measured average minimum area. $A_{min,avg}$, as given in Table 2. In the co-flow configuration, the 2× vertical coupon has slightly higher effectiveness than the 2× angled coupon. This is again the result of greater roughness in the 2× angled coupon because of the build direction. Qualitatively, the sharp increase in effectiveness is observed for $M < 1$ as well as the small decline for $M > 2$. The maximum effectiveness occurs at about $M = 1.5$ as was seen in the 1× EDM coupon data and in the adiabatic film effectiveness results presented by Schroeder and Thole [18].

Comparing co-flow data to counter-flow data, the 2× vertical film holes show a difference in performance approximately equal to the difference observed with the 1× EDM holes. This suggests that in the counter-flow configuration, there could be high velocity along the windward side of the hole that is causing greater jet detachment. Although there is more roughness in the hole of the 2× vertical holes than the 1× EDM holes (see Fig. 5), the net shape of the hole 2× vertical hole is close to that of the 1× EDM hole and is not significantly affected by the roughness. The lack of roughness on the windward surface could be why the 2× vertical coupon is exhibiting differences in performance due to the coolant supply direction. On the other hand, the 2× angled holes do not show any significant difference in performance due to the coolant supply direction. An examination of the micrographs in Fig. 5 show that the 2× angled hole has a slightly different shape because of the build direction. Additionally, it has the greatest amount of roughness on the windward side of the hole (see Fig. 5). This supports the theory that the roughness in the hole diminishes the influence of the coolant supply direction on the performance when the roughness is large enough.

Augmented effectiveness data for the 1× coupons is presented in Fig. 11 in terms of coolant flow rate per unit surface area (i.e., surface mass flux). The coolant flow rate per unit surface area is calculated using the flow rate through the three film holes in the middle of the coupon and dividing it by the area over the area over which the effectiveness is being averaged in the calculation of $\bar{\bar{\phi}}$. This approach to viewing the data exposes how effectively a certain mass flow rate of coolant is reducing the surface temperature per unit area of the coupon surface, which is arguably more

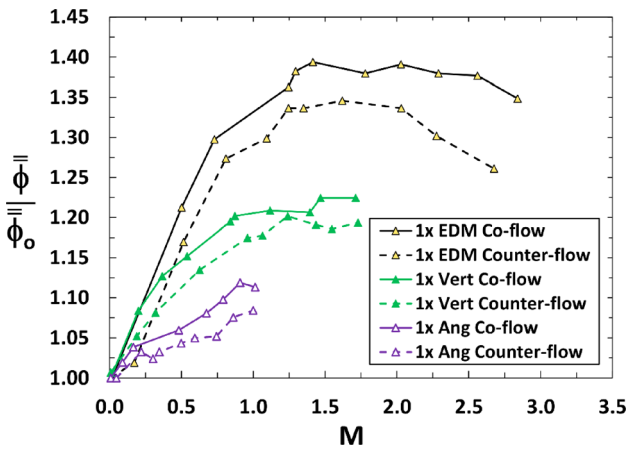

Fig. 9 Augmented area-averaged effectiveness as a function of blowing ratio for 1× coupons

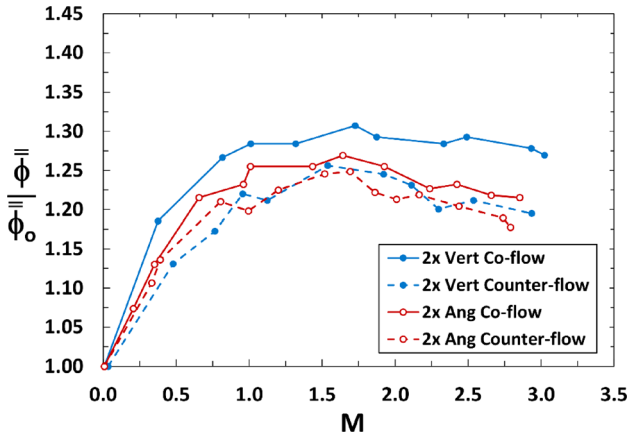

Fig. 10 Augmented area-averaged effectiveness as a function of blowing ratio for the 2× coupons

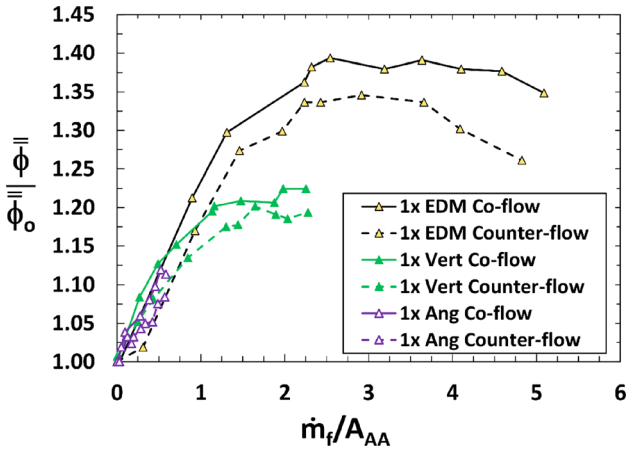

Fig. 11 Augmented area-averaged effectiveness as a function of the ratio of mass flux of the mainstream to mass flux from the coupon surface

pragmatic for a turbine designer. Ideally, one would want the highest augmented effectiveness with the lowest flow rate.

When the data are examined in terms of the surface mass flux, one can see that all 1× data series collapse when surface mass flux ratio is low. The data from the 1× angled coupon, which had a much lower augmented effectiveness at a given M than any other coupons, now aligns with the other data. The small area of the 1× angled holes contributed to a much higher M than any other coupon for a given mass flow rate. The low C_d and small area seriously restrict the amount of coolant flow possible from the 1× angled holes, which means their cooling capability is limited. The 1× vertical coupon shows more potential for cooling capabilities than the 1× angled, but still has a lower effectiveness than the 1× EDM coupon for $(\dot{m}_f/A_{AA})/(\rho_\infty U_\infty) > 0.002$. The 2× data were also examined in a similar manner, but the data did not show any notable differences when compared to Fig. 10.

Conclusions

Additive manufacturing technologies have been around for several years, but there is much research that must be done before its full potential in industrial applications can be realized. Once the impacts additive manufacturing has on performance are better understood, the enhanced design space offered by this technology can be exploited to produce truly optimized designs with fewer constraints based on manufacturing. To add to the understanding of these impacts in the context of gas turbine engines, a series of test coupons with film cooling holes fed by a small rectangular channel were made with laser powder bed fusion out of a high-temperature nickel alloy. The overall cooling performance was evaluated at engine relevant conditions over a range of operating parameters. This study was an extension of previous work done by the current authors that characterized film cooling performance of additively manufactured coupons. The unique contribution of this study was examining the discharge coefficient from additively manufactured film cooling holes and investigating the effect of coolant supply feed direction on the performance of the holes.

Discharge coefficient results showed that the discharge coefficient is a strong function of relative roughness in the hole. The smoothest holes made with additive manufacturing had a discharge coefficient of about 0.7, and the roughest had a discharge coefficient around 0.3. The low discharge coefficient was the result of very large roughness generated by the unfavorable build direction that reduced the flow area.

Overall effectiveness results showed that increased roughness in the film cooling hole results in decreased effectiveness. The additively manufactured holes with the greatest roughness gave the lowest effectiveness.

Coolant supply direction had an impact on the film performance of the 1× EDM and the 2× vertical coupons. Both coupons had lower effectiveness when coolant was being supplied in the counter-flow direction. The effectiveness results of the remaining coupons' were not affected by the coolant supply direction because of the roughness of these coupons mixed out any high velocity regions that have been shown to develop in smooth film cooling holes.

The additively manufactured film cooling holes at the 1× scale generally performed poorly with regard to effectiveness. Caution should be used when choosing such small holes in conventional designs when they are to be additively manufactured. However, holes this small may be ideal for large arrays of holes. The results showed that the film cooling performance is not much different between hole sizes when examined on the basis of total mass flux from the surface. Advantages of in-hole convection from the high roughness could make this approach a very efficient method of surface cooling.

As more studies investigate the impact of additive manufacturing on heat transfer and fluid flow systems, designers will be able to exploit new information to optimize designs for better performance. Applications of additive manufacturing for production components of gas turbine engines will become more apparent as studies like this one examine this technology's impact on part performance.

Acknowledgment

The authors would like to thank Pratt & Whitney for the financial and technical assistance throughout this study.

Funding Data

- Pratt & Whitney (00093).

Nomenclature

A_c = cross-sectional flow area of internal channel
A_{min} = minimum flow area of film cooling hole
A_{AA} = surface area of averaged region
Bi = Biot number, $h_\infty t/\kappa$
C_d = discharge coefficient
D = film hole metering section diameter
D_h = hydraulic diameter, $4A_c/p$
DR = density ratio, ρ_c/ρ_∞
FP = mass flow parameter, $\dot{m}(RT_c)^{0.5}/P_cA_c$
h = convective heat transfer coefficient
L = hole length
M = blowing ratio, $(\dot{m}_f/A_{min})/(\rho_\infty U_\infty)$
$\dot{m}$ = mass flow rate
Ma = Mach number
N = number of film cooling holes in coupon
p = wetted perimeter
P = static pressure
PR = pressure ratio
R = gas constant
R_a = arithmetic mean roughness
Re = Reynolds number, VD_h/ν
S = lateral distance between holes, pitch
t = coupon wall thickness
T = temperature
U = maximum/centerline velocity
V = mass average velocity
x = streamwise distance

Greek Symbols

γ = ratio of specific heats
δ = boundary layer thickness
δ^* = boundary layer displacement thickness

θ = boundary layer momentum thickness
η = adiabatic effectiveness
κ = thermal conductivity of coupon
ν = kinematic viscosity
ρ = fluid density
φ = overall effectiveness $(T_\infty\text{-}T_s)/(T_\infty\text{-}T_c)$
$\bar{\phi}$ = area averaged overall effectiveness
χ = coolant warming factor $(T_\infty\text{-}T_{c,exit})/(T_\infty\text{-}T_{c,in})$

Subscripts

avg = averaged
c = coolant
exit = exit of film cooling hole
f = film cooling flow
i = coupon internal channel
in = inlet to film cooling hole
o = reference condition
t = stagnation condition
∞ = mainstream

References

[1] Stimpson, C. K., Snyder, J. C., Thole, K. A., and Mongillo, D., 2016, "Roughness Effects on Flow and Heat Transfer for Additively Manufactured Channels," ASME J. Turbomach., **138**(5), p. 051008.
[2] Snyder, J. C., Stimpson, C. K., Thole, K. A., and Mongillo, D., 2016, "Build Direction Effects on Additively Manufactured Channels," ASME J. Turbomach., **138**(5), p. 051006.
[3] Stimpson, C. K., Snyder, J. C., Thole, K. A., and Mongillo, D., 2017, "Scaling Roughness Effects on Pressure Loss and Heat Transfer of Additively Manufactured Channels," ASME J. Turbomach., **139**(2), p. 021003.
[4] Kirsch, K. L., and Thole, K. A., 2016, "Heat Transfer and Pressure Loss Measurements in Additively Manufactured Wavy Microchannels," ASME J. Turbomach., **139**(1), p. 011007.
[5] Stimpson, C. K., Snyder, J. C., Thole, K. A., and Mongillo, D., 2017, "Effectiveness Measurements of Additively Manufactured Film Cooling Holes," ASME J. Turbomach., **140**(1), p. 011009.
[6] Thole, K. A., Gritsch, M., Schulz, A., and Wittig, S., 1997, "Effect of a Crossflow at the Entrance to a Film-Cooling Hole," ASME J. Fluids Eng., **119**(3), pp. 533–540.
[7] Kohli, A., and Thole, K. A., 1997, "A CFD Investigation of the Effect of Entrance Flow Conditions in Discrete Film Cooling Holes," 32nd National Heat Transfer Conference, Baltimore, MD, Aug. 8–12, pp. 223–232.
[8] Hale, C. A., Plesniak, M. W., and Ramadhyani, S., 1999, "Film Cooling Effectiveness for Short Film Cooling Holes Fed by a Narrow Plenum," ASME J. Turbomach., **122**(3), pp. 553–557.
[9] Wilkes, E., Anderson, J., McClintic, J., and Bogard, D., 2016, "An Investigation of Turbine Film Cooling Effectiveness With Shaped Holes and Internal Cross-Flow With Varying Operational Parameters," ASME Paper No. GT2016-56162.
[10] Burd, S. W., and Simon, T. W., 1997, "The Influence of Coolant Supply Geometry on Film Coolant Exit Flow and Surface Adiabatic Effectiveness," ASME Paper No. 97-GT-025.
[11] Peng, W., and Jiang, P.-X., 2012, "Experimental and Numerical Study of Film Cooling With Internal Coolant Cross-Flow Effects," Exp. Heat Transfer, **25**(4), pp. 282–300.
[12] Saumweber, C., Schulz, A., Wittig, S., and Gritsch, M., 2001, "Effects of Entrance Crossflow Directions to Film Cooling Holes," Ann. N. Y. Acad. Sci., **934**(1), pp. 401–408.
[13] McClintic, J. W., Klavetter, S. R., Winka, J. R., Anderson, J. B., Bogard, D. G., Dees, J. E., Laskowski, G. M., and Briggs, R., 2015, "The Effect of Internal Crossflow on the Adiabatic Effectiveness of Compound Angle Film Cooling Holes," ASME J. Turbomach., **137**(7), p. 071006.
[14] Klavetter, S. R., McClintic, J. W., Bogard, D. G., Dees, J. E., Laskowski, G. M., and Briggs, R., 2016, "The Effect of Rib Turbulators on Film Cooling Effectiveness of round Compound Angle Holes Fed by an Internal Cross-Flow," ASME J. Turbomach., **138**(12), p. 121006.
[15] Sakai, E., and Takahashi, T., 2011, "Experimental and Numerical Study on Effects of Turbulence Promoters on Flat Plate Film Cooling," ASME Paper No. GT2011-45196.
[16] Agata, Y., Takahashi, T., Sakai, E., and Nishino, K., 2012, "Effects of Turbulence Promoters of Gas Turbine Blades on Film Cooling Performance," J. Therm. Sci. Technol., **7**(4), pp. 603–618.
[17] Agata, Y., Takahashi, T., Sakai, E., and Nishino, K., 2013, "Effect of Orientation of Internal Turbulence Promoting Ribs on Flow Characteristics for Film Cooling," J. Therm. Sci. Technol., **8**(1), pp. 15–27.
[18] Schroeder, R. P., and Thole, K. A., 2016, "Effect of in-Hole Roughness on Film Cooling From a Shaped Hole," ASME J. Turbomach., **139**(3), p. 031004.
[19] Vinton, K. R., Nahang-Toudeshki, S., Wright, L. M., and Carter, A., 2016, "Full Coverage Film Cooling Performance for Combustor Cooling Manufactured Using DMLS," ASME Paper No. GT2016-56504.
[20] Jackowski, T., Schulz, A., Bauer, H.-J., Gerendás, M., and Behrendt, T., 2016, "Effusion Cooled Combustor Liner Tiles With Modern Cooling Concepts: A Comparative Experimental Study," ASME Paper No. GT2016-56598.
[21] Schroeder, R. P., and Thole, K. A., 2014, "Adiabatic Effectiveness Measurements for a Baseline Shaped Film Cooling Hole," ASME Paper No. GT2014-25992.
[22] EOS GmbH, 2014, "*Material Data Sheet: EOS NickelAlloy HX*," EOS GmbH, Munchen, Germany.
[23] EOS GmbH, 2011, *Basic Training EOSINT M 280*, EOS GmbH, Munchen, Germany.
[24] Reinhart, C., 2011, *Industrial CT & Precision*, Volume Graphics GmbH, Heidelberg, Germany.
[25] Kays, W., Crawford, M., and Weigand, B., 2004, *Convective Heat & Mass Transfer*, McGraw-Hill, Boston, MA.
[26] Gritsch, M., Schulz, A., and Wittig, S., 2000, "Film-Cooling Holes With Expanded Exits: Near-Hole Heat Transfer Coefficients," Int. J. Heat Fluid Flow, **21**(2), pp. 146–155.
[27] Gritsch, M., Schulz, A., and Wittig, S., 1998, "Discharge Coefficient Measurements of Film-Cooling Holes With Expanded Exits," ASME J. Turbomach., **120**(3), pp. 557–563.
[28] Albert, J. E., Bogard, D. G., and Cunha, F., 2004, "Adiabatic and Overall Effectiveness for a Film Cooled Blade," ASME Paper No. GT2004-53998.
[29] Figliola, R. S., and Beasley, D. E., 2005, *Theory and Design for Mechanical Measurements*, Wiley, Hoboken, NJ.
[30] Whitfield, C. A., Schroeder, R. P., Thole, K. A., and Lewis, S. D., 2015, "Blockage Effects From Simulated Thermal Barrier Coatings for Cylindrical and Shaped Cooling Holes," ASME J. Turbomach., **137**(9), p. 091004.